第 28 卷第 8 期
2012 年 8 月

无 机 化 学 学 报
CHINESE JOURNAL OF INORGANIC CHEMISTRY

Vol.28 No.8
1717-1723

梨形核壳结构氧化锌/银亚微米球的制备、表征及光学性能

马剑琪
(陕西理工学院化学与环境科学学院,汉中 723001)

择要：利用亚锡离子还原银离子生成的金属银沉积在合成的梨形氧化锌表面作为晶种，进一步生长银纳米粒子，制备了梨形的、核壳结构的、单分散的氧化锌/银亚微米球。利用 X 射线衍射、透射电镜、能量色散 X 射线谱、紫外可见吸收谱及光致发光谱对所制备样品的形貌、微观结构、组成和光学性能进行了表征。结果表明：(1)样品是由梨形亚微米氧化锌核和银纳米颗粒壳组成；(2)在氧化锌表面的银纳米粒子作为光激发产生的电子捕获剂提高了光产生的载流子的分离效率，在能量没有改变的情况下减少了紫外发射光的强度，淬灭了可见发射光。

关键词：氧化锌亚微米球；银纳米粒子；ZnO/Ag 核壳结构亚微米球；光学性质
中图分类号：O649 **文献标识码**：A **文章编号**：1001-4861(2012)08-1717-07

Preparation, Characterization and Optical Properties of Pear-Shaped ZnO/Ag Core-Shell Submicrospheres

MA Jian-Qi
(*School of Chemistry and Environmental Science, Shaanxi University of Technology, Hanzhong, Shaanxi* 723001, *China*)

Abstract: Pear-shaped ZnO/Ag core-shell submicrospheres with good monodispersity were prepared via a seed-mediated particle growth method, where metallic Ag particles (reduction of Ag^+ by Sn^{2+}) deposited on ZnO submicrospheres were served as seeds (nucleation sites) for the further growth of Ag nanoshell overlayer. The as-prepared samples were characterized by transmission electron microscopy, energy dispersive X-ray spectroscopy, X-ray diffraction, ultraviolet-visible absorption and photoluminescence measurement. The results demonstrate that the ZnO/Ag composites are composed of pear-shaped wurtzite ZnO submicrospheres and Ag nanoparticles. The results also indicate that the efficiency for separation of photoinduced electrons from holes is enhanced, the intensity of the UV emission is reduced without energy shifts, and the visible emission peak is quenched by Ag nanoparticles on ZnO.

Key words: ZnO submicrospheres; Ag nanoparticles; ZnO/Ag core-shell submicrospheres; optical properties

Photocatalysis is one of the most dynamic areas in modern science as its potential in solving many current environmental and energy issues [1-4]. Among semiconductor photocatalysts, in addition to the most extensively studied TiO_2, ZnO with a similar band gap (3.2 eV) has attracted much attention due to its high photosensitivity and stability. In some cases, ZnO exhibits better photocatalytic activity than that of TiO_2, SnO_2, ZrO_2, WO_3, etc., due to its higher efficiency for generation of photoinduced carriers (electron-hole pairs) [5-7]. However, the quick recombination of carriers decreases the available

收稿日期：2011-12-12。收修改稿日期：2012-05-09。
陕西省自然科学基金(No.2010JM2016)和陕西省教育厅专项 (No.2010JK469)资助项目。
E-mail：jianqima@163.com

photocatalytic efficiency, thus limiting its practical application in the environment field[8]. Depositing the semiconductor with noble metal nanoparticles (NPs) such as Ag[9], Au[10], Pt[11], and so on is one of the efficient ways to improve the capability of photochemical degradation by trapping the photoinduced carriers[12]. For example, depositing Ag nanoparticles (Ag NPs) on various kinds of micro/nano structured ZnO, such as nanoparticle, nanorod, nanofiber, hollow sphere, etc., can hinder the quick recombination of carriers and improve its photocatalytic activity[13-16]. It is widely accepted that Ag NPs on ZnO can trap the photogenerated electrons from the semiconductor and thus enhance the separation efficiency of photogenerated electrons and holes. Nonetheless, so far there have been only a few examples about the synthesis of ZnO/Ag core-shell submicrospheres[17-18]. In this work, ZnO/Ag core-shell submicrospheres, constructed by pear-shaped wurtzite ZnO submicrosphere core and Ag NPs shell, are obtained via a seed-mediated particle growth procedure, which has been used for decoration of ZnO nanorods[14], carbon nanotubes[19] and silica spheres[20]. In addition, the relation between optical properties and the separation efficiency of photoinduced carriers in the ZnO/Ag core-shell composite is investigated to evaluate the influence of deposited Ag NPs on the electronic structure and surface property of ZnO, using the as-prepared pure ZnO submicrospheres and commercial ZnO as the reference.

1 Experimental

1.1 Materials

All chemicals were analytical grade and used as received without further purification. $Zn(CH_3COO)_2 \cdot 2H_2O$(ZnAc), C_2H_5OH, $SnCl_2 \cdot H_2O$, $AgNO_3$, $NH_3 \cdot H_2O$, diethylene glycol (DEG, $HOCH_2CH_2OCH_2CH_2OH$), sodium citrate ($Na_3C_6H_5O_7$) and commercial ZnO were purchased from Shanghai Chemical Industrial Company.

1.2 Synthesis of pure pear-shaped ZnO submicrospheres

The pure pear-shaped ZnO submicrospheres used in this work were prepared by a two-stage reaction process. For the first step, 0.015 mol ZnAc was added to 150 mL DEG and heated to 160 ℃ under reflux. After 30 min, a primary reaction was performed and cooled to room temperature (RT). The product was centrifuged and the supernatant was decanted off and saved as stock solution, and the polydispersed powder was discarded. For the second step, 0.015 mol ZnAc was added to 150 mL DEG and the reaction solution was heated to 150 ℃, then 10 mL stock solution was added to the solution. Following this addition, this solution was again heated to 160 ℃, stirred for 1 h, then cooled to RT. The ZnO submicrospheres were separated from the solvent by a repeated centrifugation-sonication process.

1.3 Preparation of ZnO/Ag core-shell submicrospheres

In a typical synthesis, 50 mg of the as-prepared ZnO was dispersed into 40 mL of ethanol solution containing about 10 mg of $SnCl_2 \cdot H_2O$ with vigorous stirring for 30 min at RT and centrifuged. This resulted in sorption of Sn^{2+} onto ZnO surfaces ($ZnO@Sn^{2+}$, activated ZnO spheres). After this, the activated ZnO spheres were dispersed into 25 mL 0.005 $mol \cdot L^{-1}$ $Ag(NH_3)_2^+$ ethanol solution and stirred for about 1 h, then centrifuged to obtain ZnO spheres containing Ag seeds. The growth of Ag NPs proceeded as follows: The Ag-seeded ZnO spheres were redispersed into 25 mL aqueous solution containing 7.5 mmol $AgNO_3$ and was heated to 80 ℃, then 0.5 mL of 0.35 $mol \cdot L^{-1}$ sodium citrate was added under vigorous stirring. The solution was stirred for 60 min at 80 ℃. During the reaction, the color of the colloidal solution gradually evolved, indicating the reduction of Ag^+ by sodium citrate and the formation of the core-shell structure composites. Finally, the reaction mixture was cooled to RT and the samples were separated by a repeated centrifugation-sonication process.

1.4 Characterization

Transmission electron microscopy (TEM) images associated with energy dispersive X-ray spectroscopy (EDS) were obtained on JEOL JEM-3010 TEM with an

acceleration voltage of 200 kV. The X-ray diffraction (XRD) patterns were recorded on a Japan Rigaka D/max-IIB X-ray diffractometer equipped with a graphite diffracted-beam monochromator for Cu Kα radiation (λ =0.15418 nm) at 45 kV and 200 mA, using 0.15 mm receiving slit and scintillation counter as the detector. The 2θ region was in the range of 20°~80° with a step of 0.02° and a scanning speed of $5°\cdot min^{-1}$. UV-Vis spectra were recorded on a Hitachi U-3010 spectrophotometer. Photoluminescence (PL) spectra were recorded on a Hitachi F4500 fluorescence spectrophotometer using a Xenon lamp as the excitation source at room temperature. The samples were dispersed in ethanol using ultrasonic bath and the excitation wavelength used in PL measurement was 325 nm.

2 Results and discussion

2.1 TEM analysis

Fig.1 displays the low-magnification TEM image of pear-shaped ZnO submicrospheres and high-magnification TEM image of a single ZnO submicrosphere, respectively. Fig.1(a) reveals that the synthesized ZnO consists of monodisperse pear-shaped submicrospheres and that the average diameter of the spheres is 220 nm. Fig.1(b) shows that the single ZnO submicrosphere consists of numerous primary nanoparticles with diameters ranging from 20 to 30 nm. The size of the primary nanoparticles was too small to conclusively determine the diameter from the TEM image, therefore, the crystal size obtained from the XRD result was used as the estimated diameter (see XRD analysis).

Fig.2 shows the typical TEM images and EDS spectrum of the ZnO/Ag core-shell submicrospheres. From representative low-magnification TEM image shown in Fig.2 (a), the ZnO/Ag core-shell composites basically keep the same pear-shaped structure and monodispersity as uncoated ZnO submicrosphers with an average diameter of 250 nm. Fig.2(b) and Fig.2(c) show the high-magnification TEM images of a typical single ZnO/Ag sphere, which is assembled by many ZnO and Ag NPs. Further analysis reveals that the composite sphere is coated by uniform thin nanoshell. The nanoshell is composed of large number of spherical Ag NPs, whose size ranges from 10 nm to 30 nm. The measured average diameter of the Ag NPs is 15 nm. Only the peaks corresponding to Ag, Zn, and O are observed in the EDS spectrum (Fig.2 (d)), demonstrating once again that the samples are composed of Zn, O, and Ag, and the ZnO/Ag core-shell composites are formed. Also, one can observe a small number of free Ag NPs based on a large number of TEM images (Fig.2 (a)), showing the successful combination of Ag NPs with ZnO submicrospheres. It is worth pointing out that the Ag NPs in the composites are metallic crystalline Ag with fcc structure, which is in good agreement with the XRD result (*vide infra*).

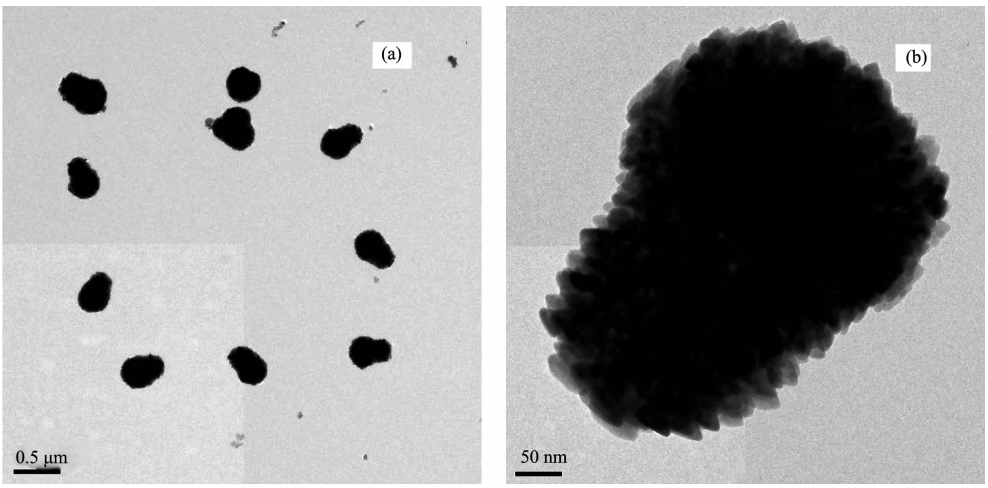

(a) Low-magnification TEM image; (b) high-magnification TEM image

Fig.1　TEM images of pear-shaped ZnO submicrospheres

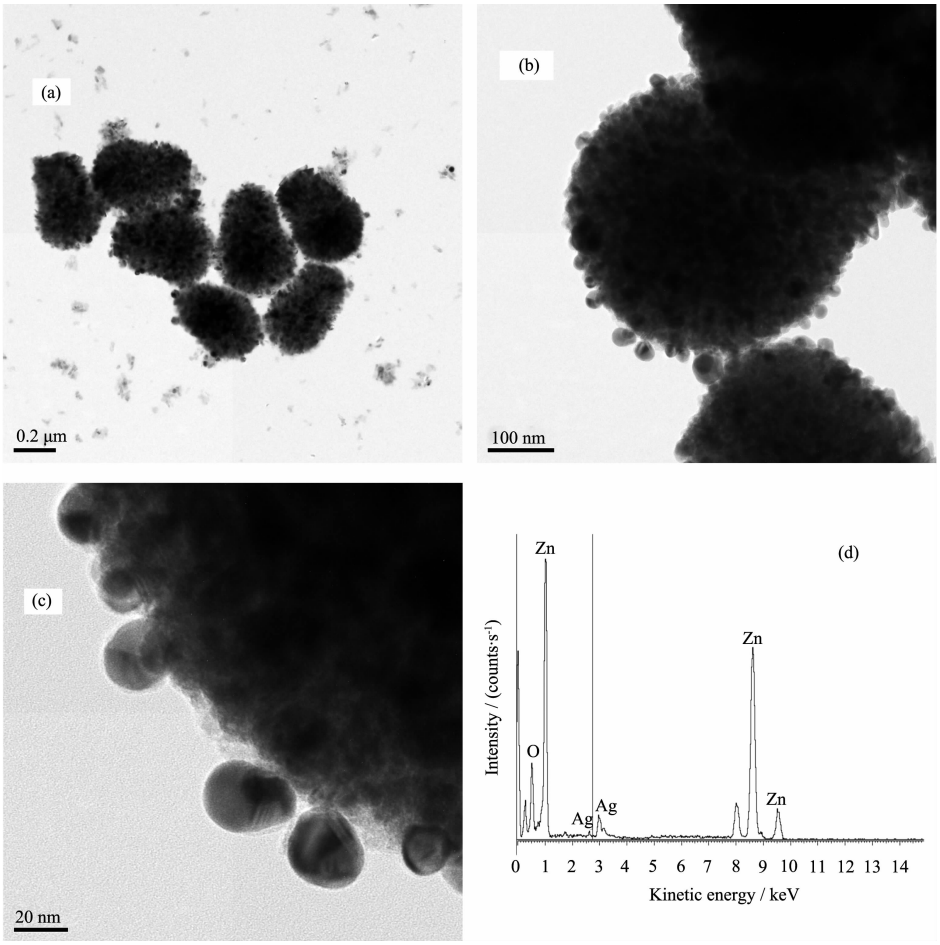

(a) Low-magnification TEM image, (b) and (c) high-magnification TEM images, (d) EDS spectrum

Fig.2 TEM images and EDS spectrum for pear-shaped ZnO/Ag core-shell submicrospheres

2.2 XRD analysis

Fig.3 shows the XRD patterns of bulk commercial ZnO, pure pear-shaped ZnO submicrospheres and ZnO/Ag core-shell submicrospheres, respectively. The peaks at 2θ=31.77°, 34.42°, 36.25°, 47.54°, 56.60°, 62.86°, and 67.81° observed in Fig.3 (a) and Fig.3(b), respectively, are indexed to the (100), (002), (101), (102), (110), (103) and (112) diffractions of ZnO crystal with a hexagonal wurtzite structure (PDF No. 36-1451). No impurity peaks are detected. However, the diffraction peaks of the ZnO submicrospheres are obviously broadened in comparison with bulk commercial ZnO due to the small particle size. As can be seen from Fig.3(c), three additional diffraction peaks appear compared to pure ZnO submicrospheres (Fig.3(b)). The three additional peaks at 2θ=38.18°, 44.42° and 64.50° (marked with

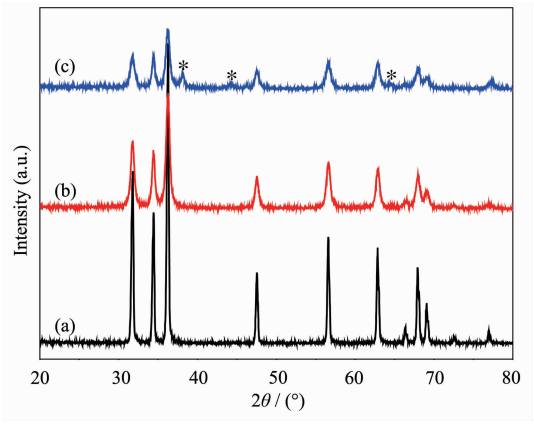

Fig.3 XRD patterns for (a) commercial ZnO, (b) pure pear-shaped ZnO submicrospheres, (c) pear-shaped ZnO/Ag core-shell submicrospheres

*) can be indexed to (111), (200), and (220) planes of fcc silver, respectively. Their position and relative intensities are in good agreement with the (PDF No.

04-0783) of bulk silver, which proves the formation of crystalline Ag. Moreover, all diffraction peak positions of ZnO in ZnO/Ag composites are in accord with that of pure ZnO submicrospheres, indicating that Ag does not incorporate into the lattice of ZnO, is only mixed with ZnO spheres. Furthermore, the average sizes of the ZnO and Ag NPs, calculated by the Scherrer formula using the strongest peaks (101) for ZnO and (111) for Ag, are estimated to be 25 and 15 nm, respectively.

2.3 Optical properties and mechanism

Fig.4 shows UV-Vis absorption spectra of bulk commercial ZnO, pure pear-shaped ZnO submicrospheres and ZnO/Ag core-shell composites. In Fig.4(a), the bulk commercial ZnO exhibits obvious UV absorption peak at 386 nm, which can be assigned to the absorption of the ZnO semiconductor. It can be easily found from Fig.4 (b) that the UV absorption position of the pear-shaped ZnO submicrospheres has a conspicuous blueshift of about 10 nm compared to that of bulk commercial ZnO due to quantum size effect[21] and the quantum confinement effect[22]. The result implies that the absorption shift of pure ZnO crystals is usually related to their size change [21-22]. As shown in Fig.4 (c), two prominent absorption peaks of the ZnO/Ag core-shell composites are observed in the UV-Vis region. The UV absorption can be assigned to absorption of ZnO submicrospheres with corresponding absorption peak at around 376 nm. The visible absorption in the range of 410~480 nm can be ascribed to the characteristic absorption of surface plasmon resulting from the metallic Ag NPs in the ZnO/Ag heterostructures[23]. The appearance of two kinds of characteristic absorption bands further confirms that the as-synthesized samples are composed of Ag NPs and ZnO submicrospheres.

Fig.5 shows PL spectra of bulk commercial ZnO, pure pear-shaped ZnO submicrospheres, and ZnO/Ag core-shell composites excited with 325 nm wavelength. In Fig.5(a), the bulk ZnO exhibits strong emission peak located at 380 nm that is attributed to the characteristic emission of semiconductor ZnO[24]. In Fig.5 (b), the pure ZnO submicrospheres exhibit a doubly peaked emission spectrum, with a strong UV band centered at 366 nm originating from the excitonic emission. The UV emission energy shifts to the high energy in comparison with that of bulk ZnO, i.e. there is a clear blue-shift. The blue-shift may be caused by the oxygen vacancies on the as-prepared ZnO spheres. The weak visible wide emission peak at around 460~480 nm is due to an electronic transition from defect-associated trap states, such as oxygen vacancies closer to the conduction band edge, to deeply trapped holes near or in the valence band[25]. Compared to the pure ZnO submicrospheres, attachment of Ag NPs to the ZnO surface reduces the intensity of the UV emission without energy shifts and quenches visible emission peak (Fig.5 (c)). The

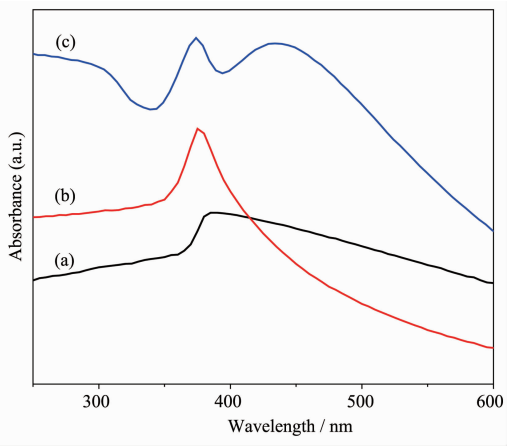

Fig.4 UV-Vis absorption spectra for (a) commercial ZnO, (b) pure pear-shaped ZnO submicrospheres, (c) pear-shaped ZnO/Ag core-shell composites

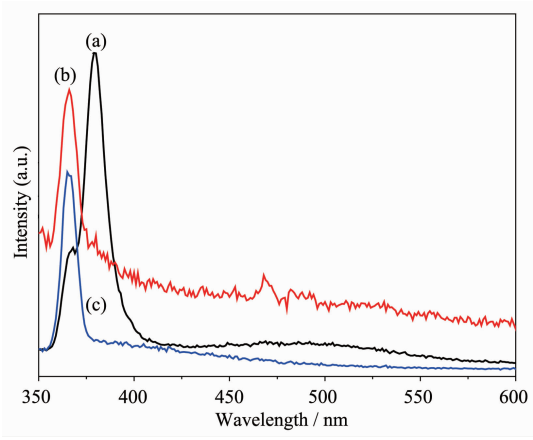

Fig.5 PL spectra for (a) commercial ZnO, (b) pure pear-shaped ZnO submicrospheres, (c) ZnO/Ag core-shell composites

intensity decrease of the UV emission for the ZnO/Ag composites can be ascribed to the electron trapping effect of Ag NPs, which act as electron acceptor, thus hindering the recombination of photogenerated carriers on ZnO. The wavelength of the visible emission peak for pure ZnO submicrospheres is in the region of the surface plasmon band of Ag NPs, and the Ag NPs absorb the emitted visible light from the ZnO spheres, thereby contributing to quenching the visible emission peak. The electron trapping effect of Ag NPs is favorable for the improvement of the photocatalytic activity of ZnO due to the enhancement of the separation efficiency of photogenerated electrons and holes. The quenching visible emission also indicates that the surface oxygen vacancies in the ZnO/Ag composites are reduced after the Ag loading, suggesting that the metallic Ag NPs are deposited on the defect sites.

The electron trapping effect of Ag NPs can be understood based on the proposed charged separation as shown in Fig.6 [16,26]. When the ZnO/Ag is illuminated by UV light with photon energy higher than the band gap of ZnO, electrons (e^-, ⊖) in the valence band (VB) can be excited to the conduction band (CB) with simultaneous generation of the same quantity of holes (h^+, ⊕) left behind. Because the bottom energy level of the CB of ZnO is higher than the new equilibrium Fermi energy level (E_f) of ZnO/Ag, the photoexcited electrons on the CB can transfer to Ag NPs from ZnO, namely, Ag NPs act as electron trapping agents and effectively hinder the recombination of photogenerated electrons and holes.

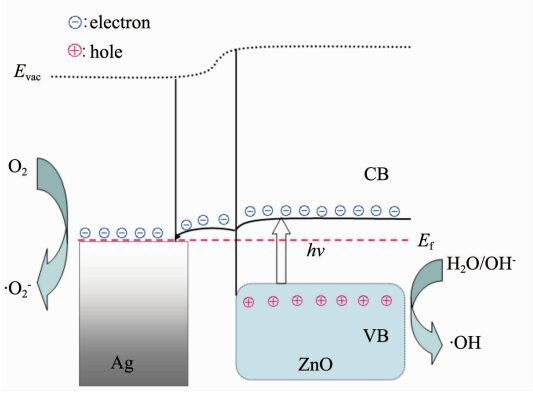

Fig.6 Proposed charge separation process for the ZnO/Ag core-shell submicrospheres

3 Conclusions

Pear-shaped ZnO/Ag core-shell submicrospheres with high stability against aggregation were synthesized. PL analysis shows that attachment of Ag NPs to the ZnO surface reduces the intensity of the UV emission without energy shifts and quenches visible emission peak. The intensity decrease of the UV emission can be ascribed to the electron trapping effect of Ag NPs, *i.e*. Ag NPs on the ZnO submicrospheres acting as electron trapping agents, enhance the separation efficiency of photogenerated electrons and holes. The reason for the quench of visible emission peak is because that the Ag NPs on the ZnO submicrospheres absorb the emitted visible light from the ZnO spheres. The enhanced separation efficiency of photogenerated electrons and holes is favorable for the improvement of the photocatalytic activity of ZnO.

References:

[1] Monteagudo J M, Durán A, Aguirre M, et al. J. *Hazard Mater.*, **2011**,**185**(1):131-139

[2] Hossain M F, Biswasc S, Zhang Z H, et al. *J. Photochem. Photobiol.* A: Chem., **2011**,**217**(1):68-75

[3] Qin Y, Wang X D, Wang Z L. *Nature*, **2008**,**451**(7180):809-813

[4] Zhang Q F, Garcia B B, Cao G Z. *J. Phys. Chem. C*, **2011**, **115**:4927-4934

[5] Sakthivel S, Neppolian B, Shankar MV, et al. *Sol. Energy Mat. Sol. C.*, **2003**,**77**(1):65-82

[6] Lu F, Cai W P, Zhang Y G. *Adv. Funct. Mater.*, **2008**,**18**(7): 1047-1056

[7] Li Y Z, Xie W, Hu X L, et al. *Langmuir*, **2010**,**26**(1):591-597

[8] LI Ben-Xia(李本侠), WANG Yan-Fen(王艳芬), WU Yu-Lei(吴玉雷). *Chinese J. Inorg. Chem.* (*Wuji Huaxue Xuebao*), **2012**,**28**:417-424

[9] Georgekutty R, Seery M K, Pillai S C. *J. Phys. Chem. C*, **2008**,**112**(35):13563-13570

[10] Li P, Wei Z, Wu T, et al. *J. Am. Chem. Soc.*, **2011**,**133**(15): 5660-5663

[11] Zeng H B, Liu P S, Cai W P, et al. *J. Phys. Chem. C*,

2008,**112**(49):19620-19624

[12] Chiou J W, Ray S C, Tsai H M, et al. *J. Phys. Chem. C*, **2011**,**115**(6):2650-2655

[13]Zheng Y H, Zheng L R, Zhan Y Y, et al. *Inorg. Chem*, **2007**,**46**(17):6980-6986

[14]Li F, Yuan Y L, Luo J Y, et al. *Appl. Surf. Sci.*, **2010**,**256**(20):6076-6082

[15]Lin D D, Wu H, Zhang R, et al. *Chem. Mater.*, **2009**,**21**(15):3479-3484

[16]Lu W W, Gao S Y, Wang J J. *J. Phys. Chem. C*, **2008**,**112**(43):16792-16800

[17]Xie J S, Wu Q S. *Mater. Lett*., **2010**,**64**(3):389-392

[18]Tian C G, Li W, Pan K, et al. *J. Solid State Chem*., **2010**, **183**(11):2720-2725

[19]Ang L M, Andy Hor T S, Xu G Q, et al. *Chem. Mater*., **1999**,**11**(8):2115-2118

[20]Kobayashi Y, Maceira V S, Marzan L M L. *Chem. Mater*., **2001**,**13**(5):1630-1633

[21]Yang Y H, Chen X Y, Feng Y, et al. *Nano Lett.*, **2007**,**7**(12):3879-3883

[22]Li Y L, Zhao X, Fan W L. *J. Phys. Chem. C*, **2011**,**115**(9):3552-3557

[23]Zhang L, Dou Y H, Gu H C. *J. Colloid Interface Sci.*, **2006**,**297**(2):660-664

[24]Zeng H B, Duan G T, Li Y, et al. *Adv. Funct. Mater*., **2010**,**20**(4):561-572

[25]Im J S, Singh J, Soares J W, et al. *J. Phys. Chem. C*, **2011**, **115**(21):10518-10523

[26]Wang X D, Summers C J, Wang Z L. *Appl. Phys. Lett*., **2005**,**86**(1):013111(3pages)